DIFFERENCE RESONANCE STUDY ON THE ELECTRON STORAGE RING ALADDIN AT SRC*

J. Liu

APS, Argonne National Laboratory and
Dept. of Physics, University of Wisconsin-Madison

E. Crosbie, L. Teng, J. Bridges
APS, Argonne National Laboratory
Argonne, IL 60439, USA

K. Symon
Dept. of Physics University of Wisconsin-Madison

W. Trzeciak
Synchrotron Radiation Center, Stoughton, WI 53589, USA

Abstract

We have studied the third-order betatron difference resonance on the electron storage ring Aladdin at SRC. The spare chromaticity correcting sextupoles were utilized to drive the desired harmonics and a pulsed kicker magnet was fired to produce the coherent oscillation of a single beam bunch. We took beam position measurements from four pairs of stripline electrodes and data acquisition devices. We observed the coupling resonance. Several typical measurements are shown. A computer program was written using multi-particle tracking to simulate the bunch motion. The simulations agree well both with analytic predictions and with the experimental results.

1 Introduction

We are conducting a series of nonlinear dynamics studies on the electron storage ring Aladdin at the Synchrotron Radiation Center, University of Wisconsin-Madison. We have concentrated initially on the third order resonances driven by sextupole errors in the magnetic field. We have presented several papers on our theoretical and experimental studies on the horizontal third-integral resonance [1, 2].

The difference resonance

$$\nu_x - 2\nu_y = m \tag{1}$$

couples the two transverse degrees of freedom. This resonance does not lead to instabilities since particle motion is bounded in both the x- and y-directions. Particle loss occurs only at the vacuum chamber walls and other physical boundaries. Near the resonance, the coupling transfers "energy" from x- to y-motion so that the y-amplitude increases periodically. The degree of coupling depends on the separation of the betatron oscillation frequencies (tunes) ν_x, ν_y from the resonance values and on the strength of the sextupole field which drives the resonance. The details of the coupling also depend on the amplitude dependence of the tunes.

In a machine such as Aladdin with four superperiods, the chromaticity correcting sextupoles can only drive resonances with $m = 4n$, where n is an integer, since they are symmetrically distributed around the ring. However, magnet misalignments and other imperfections always exist and can drive nonlinear resonances with other harmonics m. Furthermore, the second order sextupole effect and the fringe fields at quadrupole ends all contribute to the amplitude-dependent tune shifts. These tune shifts can alter the character of the resonance. In the case of unstable resonances, like the third-integral resonance, they can confine the beam within the physical aperture and make the experiments possible. In this paper, we first review the theoretical analysis of the difference resonance, then we discuss the experimental results, and finally we compare the experimental results with the results of numerical simulations. Further details can be found in Ref. [3]

2 Theoretical Analysis

For the difference resonance $\nu_x - 2\nu_y = m$, we start with the Hamiltonian in terms of action-angle variables

$$\begin{aligned} H &= \nu_x J_x + \nu_y J_y - (2J_x)^{1/2}(2J_y)B_m \cos(\gamma_x - 2\gamma_y - m\theta + \zeta_m) \\ &\quad + a J_x^2 + 2b J_x J_y + c J_y^2 , \end{aligned} \tag{2}$$

where B_m and ζ_m give the amplitude and phase of the sextupole parameter defined as

$$B_m e^{i\zeta_m} = \sum \frac{B''l}{16\pi B\rho} \beta_x^{1/2} \beta_y e^{i(\psi_x - 2\psi_y + m\theta)} . \tag{3}$$

The summation is over all sextupoles in the ring. All other symbols have their conventional meanings. In Eq. (2) the first two terms correspond to the linear motions, the third is the resonance term, and the rest are fourth order tune shift terms specified by the parameters a, b, and c.

In order to transform away the θ dependence, we take the generating function

$$W(J_1, J_2, \gamma_x, \gamma_y; \theta) = J_1(\gamma_x - 2\gamma_y - m\theta + \zeta_m) + J_2\gamma_y , \tag{4}$$

With this function, the action-angle variables are transformed according to

$$J_x = \frac{\partial W}{\partial \gamma_x} = J_1 , \tag{5}$$

$$J_y = \frac{\partial W}{\partial \gamma_y} = J_2 - 2J_1 , \tag{6}$$

$$\gamma_1 = \frac{\partial W}{\partial J_1} = \gamma_x - 2\gamma_y - m\theta + \zeta_m , \tag{7}$$

$$\gamma_2 = \frac{\partial W}{\partial J_2} = \gamma_y , \tag{8}$$

and we get a new Hamiltonian in the form

$$\begin{aligned} \mathcal{H} &= \epsilon J_1 + \nu_y J_2 - 2(2J_1)^{1/2}(J_2 - 2J_1)B_m \cos\gamma_1 \\ &\quad + aJ_1^2 + 2bJ_1(J_2 - 2J_1) + c(J_2 - 2J_1)^2 , \end{aligned} \tag{9}$$

where

$$\epsilon = \nu_x - 2\nu_y - m \tag{10}$$

is the separation of the tunes from the resonance values. We have two constants of the motion, $\mathcal{H}$ and J_2, resulting from the fact that neither θ nor γ_2 appears in $\mathcal{H}$. According to Eqs. (5) and (6), the constant J_2 is given by

$$J_2 = 2J_x + J_y . \tag{11}$$

This equation shows that both x- and y-motions are limited in maximum amplitude, and that J_x must decrease when J_y increases.

The entire motion can now be represented by the *Poincaré* map in the $\gamma_1 J_1$ phase plane, which we will call the *resonance* phase plane (see Figure 1). According to Eq. (6), for a fixed value of J_2, the motion is confined to the region inside the circle $2J_1 = J_2$ in the phase plane. On the limiting circle, the Hamiltonian (9) has the value

$$\mathcal{H} = (\frac{\epsilon}{2} + \nu_y)J_2 + \frac{a}{4}J_2^2 . \tag{12}$$

3

If we substitute this value for $\mathcal{H}$ in Eq. (9), the resulting equation factors into the product of two circles:

$$[2J_1 - J_2][A(2J_1) + 2B(2J_1)^{1/2}\cos\gamma_1 + C] = 0 , \tag{13}$$

where

$$A = a/4 - b + c , \quad B = B_m , \quad C = \epsilon/2 + (a/4 - c)J_2 . \tag{14}$$

It is useful to introduce the rectangular coordinates

$$Q = (2J_1)^{1/2}\cos\gamma_1 , \quad P = (2J_1)^{1/2}\sin\gamma_1 , \tag{15}$$

in terms of which Eq. (15) can be written

$$[P^2 + Q^2 - J_2][A(P^2 + Q^2) + 2BQ + C] = 0 . \tag{16}$$

Setting the first factor to zero, we get the limiting circle $2J_1 = J_2$. Setting the second factor to zero gives the dividing circle which is centered on the Q-axis at

$$Q_c = -B/A \tag{17}$$

and has the radius

$$R = \frac{1}{A}\sqrt{B^2 - AC} . \tag{18}$$

The dividing circle crosses the Q-axis at the points

$$Q_1 = Q_c \mp R , \quad \text{and} \quad Q_2 = Q_c \pm R , \tag{19}$$

where the upper sign is used if Q_c is positive, and the lower if it is negative. In the limit of small nonlinearities, when a, b, c are small, the radius R becomes large, and

$$Q_1 \doteq \pm\frac{C}{2B} , \tag{20}$$

while Q_2 becomes large. The character of the *Poincaré* map depends on the relative sizes and positions of the two circles. In Figure 1 we show three typical cases when the dividing circle is larger than the limiting circle. We have taken all parameters ϵ, A, B, C corresponding to Aladdin experiment to be described later, but the cases are not essentially different for other signs. The difference resonance is most pronounced for motions in which the y amplitude is initially very small. In the resonance phase plane the initial motion is then very close to the limiting circle. In that case, the radius of the limiting circle is determined primarily by the initial x amplitude:

$$J_2 \doteq 2J_{x0} . \tag{21}$$

In cases (a) and (c) in Figure 1 the motion remains close to the limiting circle, and the y amplitude remains small, so there is no resonant coupling. In case (b) the two

4
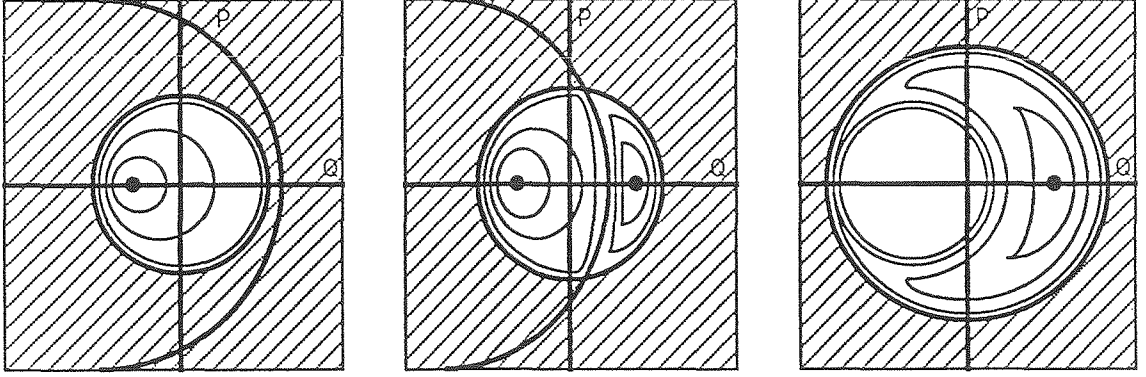
(a) $Q_1 < -\sqrt{J_2}$ (b) $-\sqrt{J_2} < Q_1 < \sqrt{J_2}$ (c) $Q_1 > \sqrt{J_2}$

Figure 1: Resonance phase plane maps

circles intersect, and the motion cannot remain near the limiting circle, but moves past the fixed point where the circles intersect and along the dividing circle. This is the case of resonant coupling. The y amplitude increases to a maximum near the intersection $Q = Q_1$ of the dividing circle with the Q-axis. The maximum y amplitude is given approximately by

$$\sqrt{2J_{y\mathrm{max}}} \doteq \sqrt{2(2J_{x0} - Q_1^2)}. \tag{22}$$

Since the phase point remains for a long time near the fixed point where the circles intersect, we expect the y motion to consist of long periods of very small amplitude, with periodic peaks. During these peaks, the x amplitude drops to a minimum given by $|Q_1|$. When $\epsilon = -2(a/4 - c)J_2$, we have complete coupling; the x amplitude drops to zero at the peaks while the y amplitude reaches a maximum with $J_{y\mathrm{max}} = J_2$.

The threshold x amplitude for resonant coupling is given by $\sqrt{2J_{x0}} = |Q_1|$. If the initial value of J_x is below this threshold, given approximately by Eq. (20), then no resonant coupling occurs. Since Q_1 depends also on J_{x0} because of the nonlinear term in the parameter C [Eq. (14)], there is also an upper threshold x amplitude, above which the nonlinearities move the tunes away from the resonance.

The "energy exchange" time, namely the time J_1 takes to complete a cycle can be shown to be much less than the synchrotron radiation damping time in Aladdin, so that we expect to be able to see more than one full coupling cycle.

3 Experimental Arrangement and Measurement

Aladdin is a 1 GeV electron storage ring which is composed of four sectors as shown in Figure 2. In normal operation it stores 15 beam bunches with transverse beam sizes $\sigma_x \simeq 0.8$mm, $\sigma_y \simeq 0.3$mm. Table 1 shows its operating parameters at the energy of 800 MeV.

Table 1: Aladdin parameters at 800 MeV

Energy	800 MeV
Circumference	88.9 m
Revolution period	300 nsec
Betatron tunes	7.14,7.23 (ν_x,ν_y)
Emittance	0.10π mm-mrad
RF harmonic number	15
RMS beam bunch length	87 mm (0.29 nsec)
Synchrotron radiation energy	17.4 keV/turn
Synchrotron radiation damping time	26.6 msec (89000 rev.)
Beam current	10 mA /bunch

In this experiment, we kept only one beam bunch in the ring and knocked out other bunches.

Hardware. In the Aladdin ring, there are 4 pairs of unused chromaticity correcting sextupoles labeled SF1/SD1, SF4/SD4, SF7/SD7, and SF10/SD10, all at high β locations. The phase advance between SF and SD is about 30°. Thus these sextupoles can be powered to give any desired harmonic at any phase.

A fast kicker magnet is used to kick the beam bunch horizontally and drive the coherent x oscillation. The kicker also drives a very small coherent vertical oscillation. This was initially inadvertent, but fortunate, since this coherent vertical oscillation can be detected by the vertical beam position monitors. The kicker is made of ferrite with a one turn coil. It can be pulsed for a total length of 350 nsec with a flat top of 150 nsec.

Four stripline-electrode beam position monitors (BPM's)are located at the quadrupoles QF9, QD9 and Q1, Q2. They measure horizontal and vertical displacements of the beam centroid, X_1, X_2 and Y_1, Y_2, respectively. Knowing the amplitude functions β_x, β_y and the phase advance between locations 1 and 2, one can then calculate the displacements and slopes at location 1.

Four two-channel ADC digitizers collect the BPM signals from the stripline electrodes. The ADC's are clocked by the RF synthesizer and triggered by the kicker
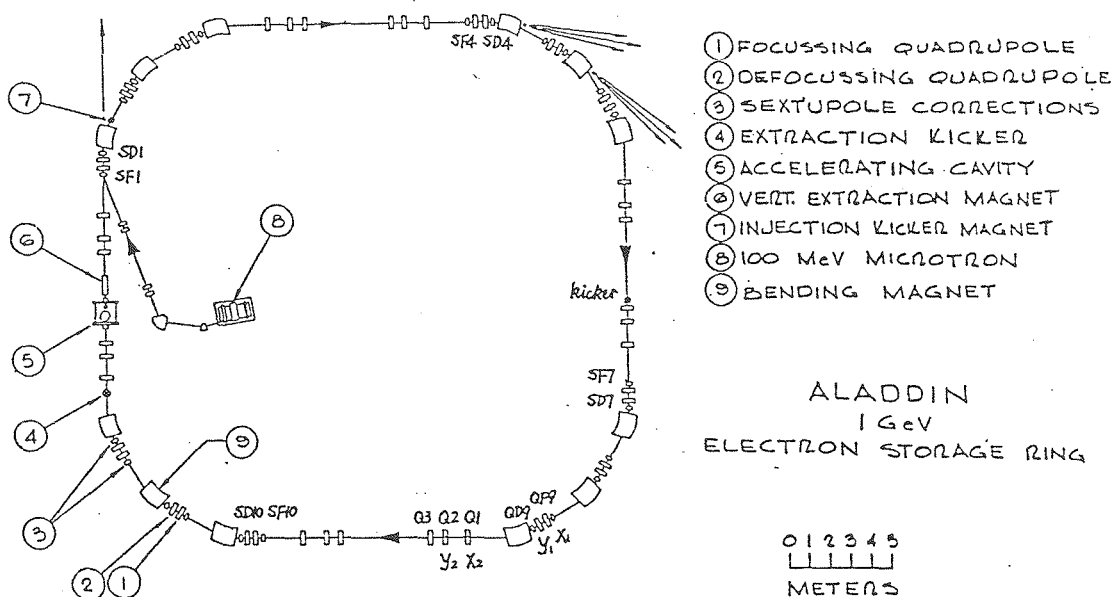
Figure 2: Aladdin configuration

magnet trigger. The data acquisition circuit must be carefully timed so that the maximum beam signal from the single circulating beam bunch can be detected. Figure 3 shows a block diagram of the data acquisition circuit.

Data acquisition. For this experiment, only one beam bunch is used and the other 14 bunches are knocked out by the RF knockout technique. Before starting a set of measurements, the closed orbit distortions are corrected to better than 20 μm by adjusting the steering magnets and the chromaticity is set to a small positive value to avoid the head-tail instability. We use as small a chromaticity as possible, to minimize the tune spread in the beam bunch.

The most easily accessible difference resonance is $2\nu_y - \nu_x = 7$. The operating tunes are moved close to the resonance by adjusting the quadrupoles manually. The 7th harmonic resonance should not be driven if the 4-fold symmetry of the Aladdin lattice were perfect. However, we found the resonance immediately, an indication that there are sizable sextupole errors in the Aladdin lattice. Since we wished to control the size of the sextupole driving term, we first tried to compensate the sextupole errors initially present. As the horizontal or vertical tune is varied, the coupling resonance can be seen as a sudden increase in vertical amplitude observed on a TV monitor connected to a camera which is focussed on the synchrotron radiation from the beam. According to formula (20) the amplitude of the driving term is approximately proportional to the tune width of the resonance. It was relatively easy to adjust the spare
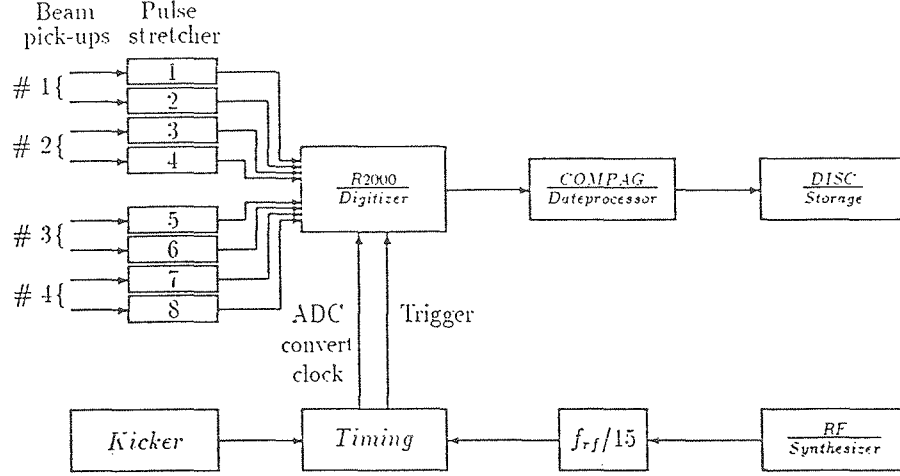
Figure 3: Block diagram of the data acquisition circuit

sextupoles SD7 and SD10 to minimize the tune width. The compensation was nearly complete with SD7 and SD10 excited by currents of 7.5 A, and -22.5 A, respectively. These large currents indicate a relatively large sextupole error somewhere in the Aladdin lattice. In the measurements, we changed either SD7 or SD10 or both, starting from these reference values, to drive the desired sextupole harmonic. The fast kicker magnet is then fired to give the beam bunch an initial controllable amplitude in the horizontal plane. After about a 25 turn delay, the digitizers take data for 4096 turns.

With the measured displacements z_1 and z_2, one can calculate the slope of the beam centroid using the formula

$$p_{z1} = [\sqrt{\beta_{z1}/\beta_{z2}}z_2 - z_1 \cos\phi_{21}]/\sin\phi_{21} , \qquad (23)$$

where $z = x$ or y, and $\phi_{21} = \phi_2 - \phi_1$ is the phase difference between the BPM's which measure z_1 and z_2. The displacement of the beam centroid is measured in BPM units, defined by

$$z = \frac{V_a - V_b}{V_a + V_b} \text{ (BPM's)} , \qquad (24)$$

where the V's are signals derived from the stripline electrode pairs through a diode-LC stretch filter. For Aladdin, we have 1 BPM = 18.9 mm, which is the minor radius of the vacuum chamber. Figure 4 shows a typical set of measured data. We plot x and y versus turn number; we also show the frequency spectra of x and y. The operating tunes correspond to $\epsilon = -0.0044$ [Eq. (10)]. The first coupling peak occurs at about the 275th turn and $|y_{max}|/|x_0| = 0.70$, where $|x_0|$ is the initial horizontal amplitude. From the spectra, we can find the nonlinear coupling peaks. The tunes
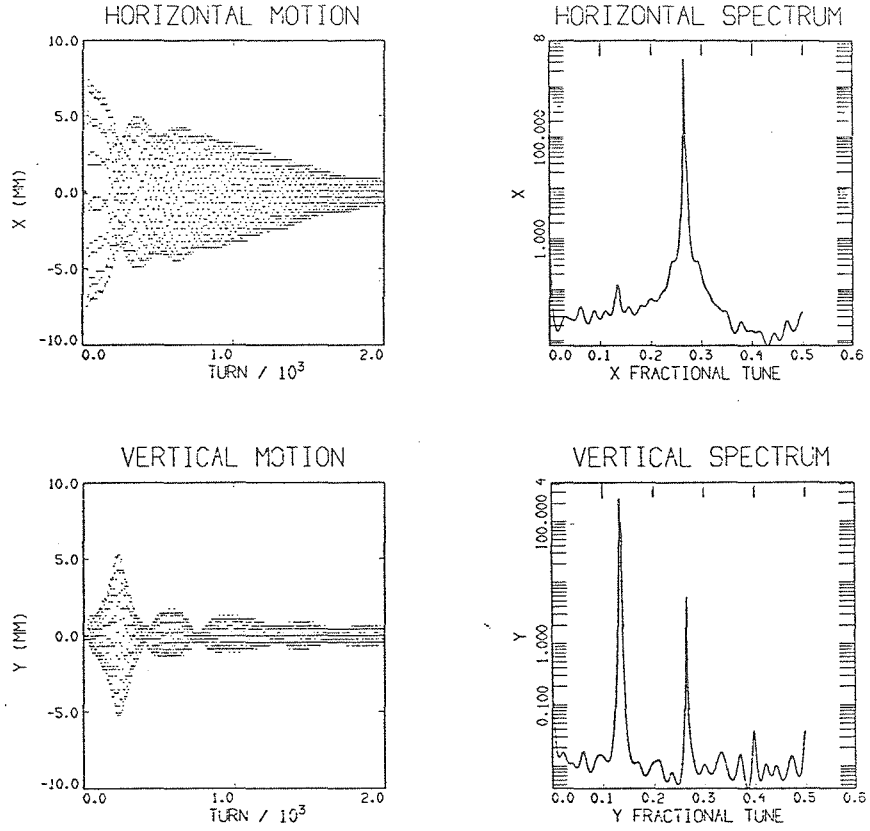
8

Figure 4: Experimental measurements at $\nu_x = 7.266$, $\nu_y = 7.135$, with sextupole currents SD7: -7.5 A, SD10: 22.5 A.
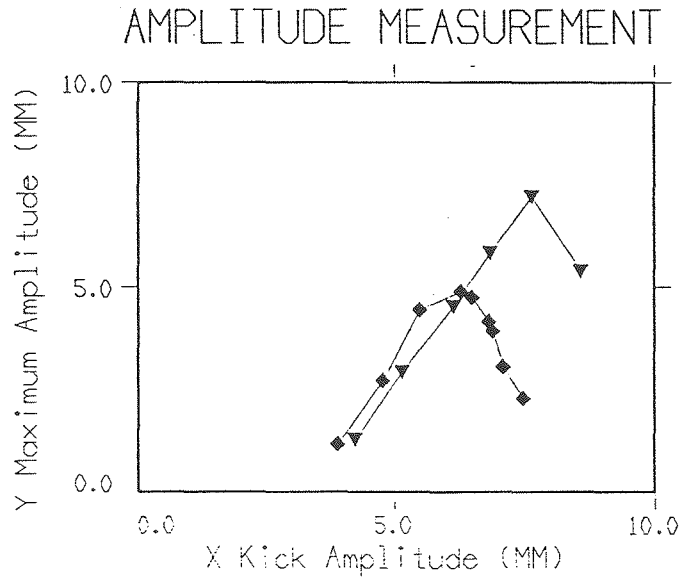

Figure 5: Peak y amplitude versus initial x amplitude

9

are rather strongly amplitude dependent due to the second order sextupole effects and effects of the fringe fields at quadrupole ends. Figure 5 shows two plots of measured $|y_{max}|$ versus $|x_0|$ at two different sextupole settings. The threshold in $|x_0|$ is clearly shown, and the curves suggest that there is also an upper limit as predicted in the previous section.

4 Simulation

Computations of the motion of a single particle through the Aladdin lattice confirm the analytical results presented in Section 2 in all respects. In Figure 6 we show the computed x and y motions plotted versus turn number for a typical case above threshold. They correspond to what we deduced from Figure 1(b), for motion with a small initial y amplitude. We also show in Figure 6(c) the *Poincaré* map in the resonance phase plane for the computed orbits, for comparison with Figure 1(b).

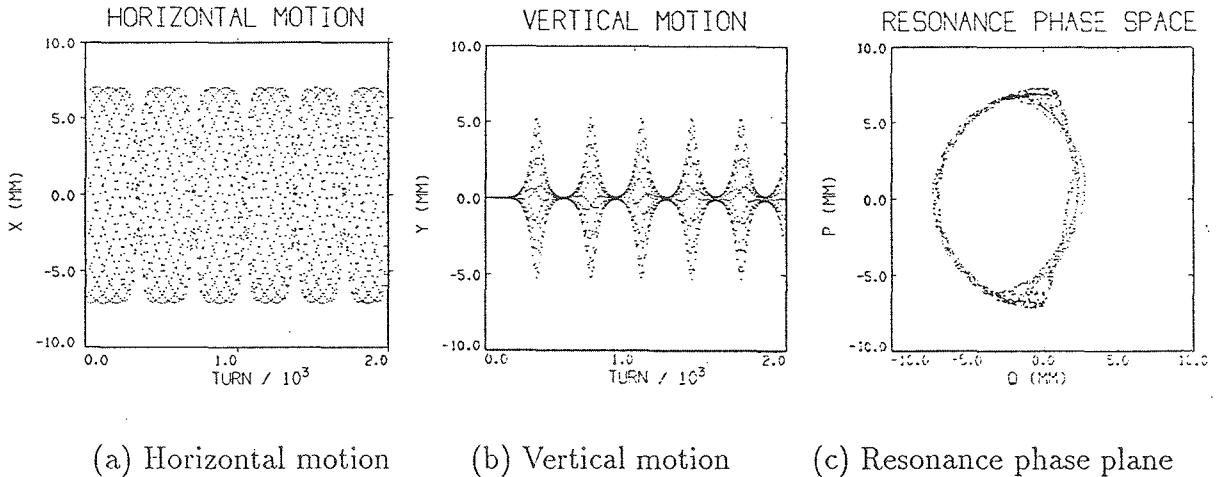(a) Horizontal motion   (b) Vertical motion   (c) Resonance phase plane

Figure 6: Computed motion of a single particle

The single-particle results suggest but do not match exactly the experimental results in Figure 4. The experimental results represent the centroid of the beam bunch containing about 10^{10} electrons. After the kicker is fired the beam centroid does indeed reach a minimum in x and a maximum in y within a few hundred turns. However, due to the amplitude dependence of the tunes, particles tend to spread out over the phase space in such a way that the beam centroid exhibits a damped oscillatory motion.

In order to simulate this diagnostic effect, a computer code was developed to track the motion of the centroid of a bunched beam. This code uses the following

algebraic transformation:

$$Z_{j+1} = Z_j \cos \phi_{zj} + P_{zj} \sin \phi_{zj} ,$$
$$P_{zj+1} = -Z_j \sin \phi_{zj} + P_{zj} \cos \phi_{zj} + \Delta P_{zj} , \qquad (25)$$

where Z and P_z are defined as $Z = z/\sqrt{\beta_z/\beta_{z0}}$, $P_z = (\beta_z p_z + \alpha_z z)/\sqrt{\beta_z/\beta_{z0}}$, and ΔP_{zj} is the kick from nonlinear magnet elements:

$$\Delta P_z = -\sqrt{\beta_z \beta_{z0}} \left(\frac{\Delta B \ell}{B\rho} \right)_z , \qquad (26)$$

and the multipole components of the magnetic field are given by

$$\frac{(\Delta B_x + i\Delta B_y)\ell}{B\rho} = \sum_n \frac{1}{n!} \frac{B^{(n)}\ell}{B\rho} (x + iy)^n . \qquad (27)$$

Using this transformation, one can carry the particle tracking from one nonlinear element to another. The linear lattice parameters are derived from the program COMFORT. The amplitude dependencies of the tunes due to the fringe fields of the quadrupole ends are simulated by appropriate octupoles. Three octupoles are included in each superperoid and have strengths given by our present best evaluations. The sextupole and octupole terms are included in the code as nonlinear bumps. The beam size is represented by a Gaussian distribution in the initial X and P_x phase space. The coordinates of the centroid are then calculated after each turn. In accordance with the experimental conditions, we have set the initial y values very small for all particles. Figure 7 shows the simulation results corresponding to the measurements shown in Figure 4. The first coupling peak occurs at about 300th turn and it gives $|y_{\max}|/|x_{\max}| = 0.71$. Those octupole components damp the oscillations of the beam centroid and contribute to the nonlinear tune shifts. The simulated results agree rather well with the experimental measurements, showing all the observed features with roughly the correct magnitudes. It has not been possible to extract the resonance phase plane coordinates from the experimental data, because they depend sensitively on the relative magnitudes and phases of the x and y oscillations.

We plan to continue our studies on this and other nonlinear resonances in Aladdin, using a newly developed kicker magnet which can produce controlled initial beam displacements in both the horizontal and vertical directions.

References

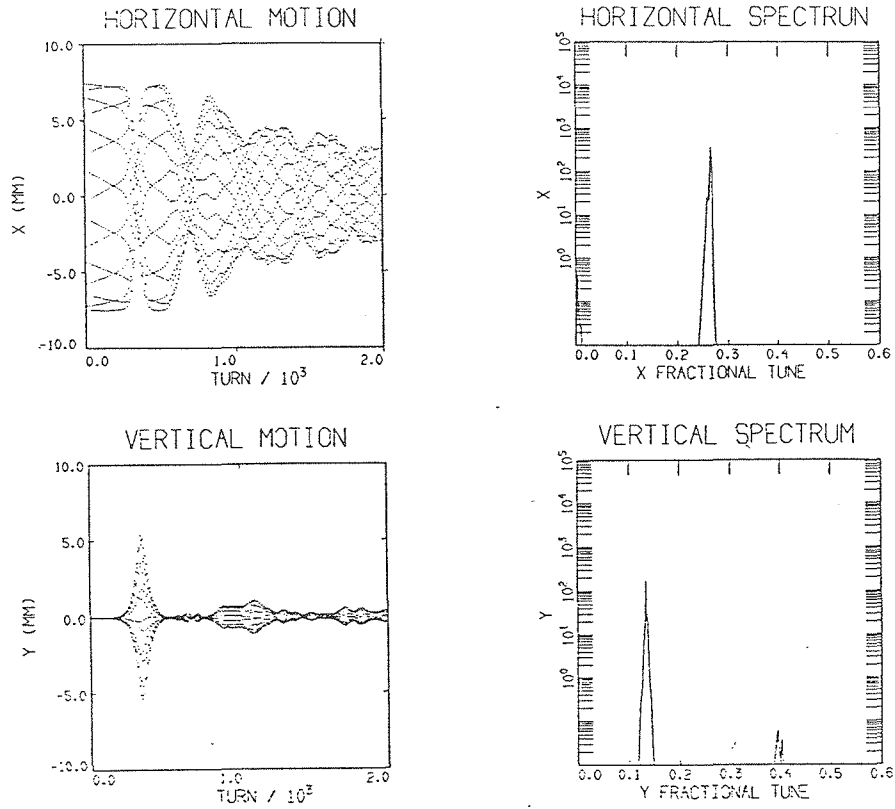[1] J. Bridges, et al. Particle Accelerators, Vol. 28, 1, 1990.

Figure 7: Simulation results for $\nu_x = 7.266/\nu_y = 7.135$, 100 particles

[2] E. Crosbie, et al. "Non-linear Resonance Studies at the Synchrotron Radiation Center, Stoughton, Wisconsin", Particle Accelerator Conference, San Francisco, 6-9 May, 1991.

[3] J. Liu, "Investigation and Simulation of Nonlinear Dynamics in ALADDIN", MS thesis, University of Wisconsin-Madison, 1989.